

## Decay modes of the isoscalar giant quadrupole resonance in the Zn isotopes

M. T. Collins,\* C. C. Chang, and S. L. Tabor†

*Department of Physics and Astronomy, University of Maryland, College Park, Maryland 20742*

(Received 5 November 1980)

Particle-particle coincidence measurements have been performed to study directly the particle decay modes of the isoscalar giant quadrupole resonance in  $^{64}\text{Zn}$ ,  $^{66}\text{Zn}$ , and  $^{68}\text{Zn}$ . The resonance was excited via inelastic alpha particle scattering at 160 MeV and decay protons, neutrons, and alpha particles were detected in coincidence at a number of angles. The importance of statistical processes in the decay of the giant quadrupole resonance is shown by the similarity of the measured branching ratios to statistical model predictions, which vary systematically across the Zn isotopes. This result is consistent with exciton model calculations which predict that the giant quadrupole resonance width in Zn isotopes is predominantly a spreading width rather than an escape width.

[ NUCLEAR REACTIONS  $^{64}\text{Zn}(\alpha,\alpha x)$ ,  $^{66}\text{Zn}(\alpha,\alpha x)$ ,  $^{68}\text{Zn}(\alpha,\alpha x)$ ,  
 $x = p, n, \alpha$ ,  $E_\alpha = 160$  MeV; measured  $d^4\sigma/d\Omega_\alpha d\Omega_x dE_\alpha dE_x$ ; de-  
 deduced giant quadrupole resonance branching ratios; compared with  
 branching ratios calculated in statistical model. ]

## I. INTRODUCTION

The isoscalar giant quadrupole resonance (GQR) has been observed in a wide variety of nuclei through inelastic scattering using such projectiles as the electron, pion, light and heavy ions.<sup>1-9</sup> The systematics of the GQR excitation energy and width have been established through alpha particle scattering. A survey of 96 and 115 MeV inelastic alpha particle scattering has revealed a GQR peak in nuclei in the mass range  $32 \leq A \leq 208$ .<sup>5</sup> Studies at higher alpha particle bombarding energies have identified the GQR in systems lighter than mass 32, such as  $^{28}\text{Si}$  and  $^{16}\text{O}$ .<sup>10,11</sup> However, the GQR has not been located in  $^{12}\text{C}$ .<sup>12</sup> The resonance appears at an excitation energy of about  $63A^{-1/3}$  MeV, except for the lightest systems, where it is located at slightly lower energies. The GQR widths decrease with increasing mass number from about 6 MeV in  $^{16}\text{O}$  to 2.6 MeV in  $^{208}\text{Pb}$ . Also, the GQR seen in the lighter elements exhausts from 30–60% of the isoscalar electric quadrupole energy weighted sum rule (EWSR), while in the heaviest elements it exhausts essentially all of the EWSR strength.

Various macroscopic and microscopic theories have been advanced to describe the systematics of giant resonances. (For an extensive list see Ref. 13.) For example, a recent macroscopic theory describes

the isoscalar giant resonances as the motion of a viscous fluid within deformable boundaries.<sup>13</sup> Good fits are obtained for the GQR energy as a function of mass, but the widths are generally underestimated. The microscopic theories of giant resonances have also had some difficulty in accounting for the resonance widths. Calculations for spherically symmetric nuclei, such as  $^{16}\text{O}$ ,  $^{40}\text{Ca}$ , and  $^{208}\text{Pb}$ , have shown that the large resonance widths cannot be predicted unless multiparticle, multihole states are included along with the simple one-particle, one-hole (1p-1h) GQR configurations.<sup>14-16</sup>

In an independent particle harmonic oscillator picture, the GQR is initially excited as a superposition of 1p-1h states in which the particle is promoted by two oscillator shells. If the state immediately decays by emitting a particle, this process is characterized by an "escape width,"  $\Gamma^\dagger$ . If the GQR proceeds through more complex particle-hole states (2p-2h, 3p-3h, etc.), before decaying, this is described by a "spreading width,"  $\Gamma^\ddagger$ . The total width of the state is the sum of the partial widths of its various decay modes. It is therefore necessary to study the decay properties of the GQR to learn more about its structure and to understand the origin of its width.

The strong excitation of the GQR in inelastic hadron scattering has made direct particle-particle

coincidence measurements of the GQR decay feasible. Such experiments have now been performed on several nuclei from  $^{12}\text{C}$  to  $^{62}\text{Ni}$ .<sup>10-12,17-20</sup> Some coincidence work has been done to look for giant resonance neutron decay or fission decay in the mass region of  $^{208}\text{Pb}$  and above, but the experimental picture is not firmly established at this time.<sup>21-23</sup> The results of GQR charged particle decay experiments done at Texas A&M on  $^{40}\text{Ca}$  (Ref. 17) and at Maryland on  $^{58}\text{Ni}$  (Ref. 18) indicate the possibility of a statistical decay process. It was suggested that a study of nuclei with quite different particle decay thresholds and penetrabilities was needed to determine the extent of the influence of statistical effects on the decay.<sup>18</sup> We present here the results of a coincidence experiment designed to look for the strong isotopic (particle emission threshold) dependence of the GQR decay in  $^{64}\text{Zn}$ ,  $^{66}\text{Zn}$ , and  $^{68}\text{Zn}$  which is predicted by Hauser-Feshbach calculations. The total proton, neutron, and alpha particle decay branching ratios of the GQR peak and the underlying nuclear continuum have been measured and these will be compared with statistical model predictions.

## II. EXPERIMENTAL PROCEDURE

The experimental arrangement for the GQR particle decay measurements is shown schematically in Fig. 1. The GQR was excited through 160 MeV alpha particle scattering detected at  $14^\circ$  in the lab, near the third maximum in the angular distribution of the GQR in Zn. At this angle, the nuclear continuum underlying the resonance was rather flat

while the GQR cross section remained adequate. Low energy decay particles were analyzed in secondary charged particle detector telescopes (labeled D) or a neutron counter (labeled N). Each decay particle telescope was placed in coincidence separately with each of two independent scattered particle detectors (labeled S) using standard fast timing logic. The scattered particle detectors were located at equal angles on opposite sides of the beam, which provided a total of six coincidence angle pairs per run. The inelastic alpha particle singles spectra from  $S1$  and  $S2$  were also taken during the runs.

All targets were isotopically enriched, self-supporting foils of the order of  $1 \text{ mg/cm}^2$  in thickness. The target angle shown in Fig. 1 was chosen to reduce the effective target thickness for the low energy decay charged particles. Beam currents were limited to between 10 and 20 nA, which resulted in a real to random charged particle coincidence rate of about 4 to 1 in the region of the GQR.

Charged particles were detected in conventional  $\Delta E$ - $E$  solid state counter telescopes. Each scattered alpha particle system consisted of a 1 mm Si  $\Delta E$  detector followed by a 5 mm Si(Li)  $E$  detector turned to an angle of  $60^\circ$  to increase the effective detector thickness. The solid angles for the two scattered alpha particle systems were about 2 msr, with angular acceptances of about  $2^\circ$ . The low energy decay charged particles were essentially limited to protons and alpha particles. These were detected in a system with a  $28 \mu\text{m}$  Si  $\Delta E$  detector and a 2 mm Si(Li)  $E$  detector. A  $500 \mu\text{m}$  Si detector was used to reject any high energy particles that passed through the first two counters. The recoil nuclei and a small number of very low energy protons and

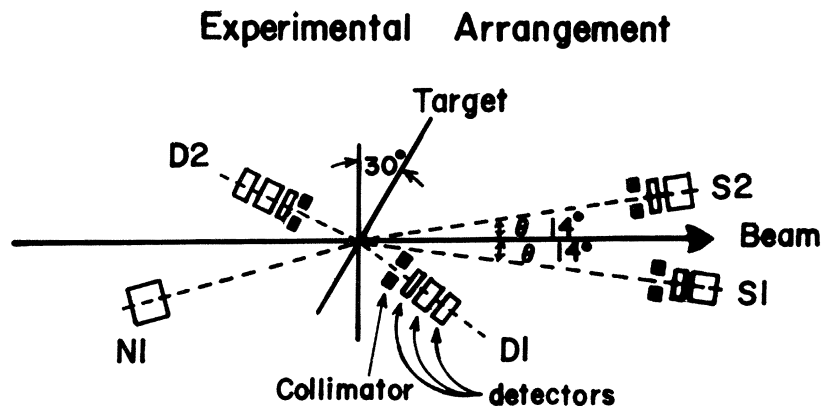


FIG. 1. The experimental setup for the GQR decay coincidence experiment.

alpha particles were stopped in the  $\Delta E$  detector and were identified by time of flight. The two decay particle solid angles were about 10 msr and the angular acceptances of the order of  $6^\circ$ .

The decay neutron detector was a 5 in.  $\times$  5 in. cylindrical NE-102 plastic scintillator. The detector was unshielded and neutron-gamma ray separation was made through time of flight relative to the scattered alpha particle detector. It was placed just outside of the 0.76 cm thick scattering chamber wall and the estimated 3–5% neutron attenuation in the wall was neglected. The solid angle and angular acceptance were approximately 15 msr and  $8^\circ$ , respectively. The neutron detector threshold was estimated from the position of the Compton edge of a  $^{137}\text{Cs}$  source. Detector efficiencies as a function of neutron energy and detector threshold setting were calculated by Kalenda using the Monte Carlo technique of Ref. 24. The effective detector efficiency in the energy range of the detected neutrons was estimated to be  $54 \pm 20\%$ .

### III. DATA ANALYSIS AND RESULTS

The experiment was designed to measure the proton, neutron, and alpha particle decay branching ratios of the GQR in  $^{64}\text{Zn}$ ,  $^{66}\text{Zn}$ , and  $^{68}\text{Zn}$ . Only the total GQR particle decay branching ratios were measured since previous results<sup>18</sup> from the GQR decay in  $^{58}\text{Ni}$  showed that the resonance decay to specific final states could not be distinguished from that of the continuum background.

The differential cross section of the GQR from 160 MeV inelastic alpha particle scattering at  $14^\circ$  was measured for each isotope simultaneously with the coincidence data. The singles spectra are shown as parts (a) of Figs. 2–4. The GQR is visible for all three isotopes as a broad peak centered at about 15.5 MeV and resting on a large nuclear continuum. A carbon-hydrogen contaminant spectrum has been subtracted from all of the Zn spectra. Based on the  $^{12}\text{C}$  ground state strength in the Zn singles spectra before subtraction, it was estimated that  $^{12}\text{C}$  contamination contributed 7%, 4%, and 3% to the yield found in the GQR regions of  $^{64}\text{Zn}$ ,  $^{66}\text{Zn}$ , and  $^{68}\text{Zn}$ , respectively.

The GQR shapes and strengths look very similar in the three  $^{12}\text{C}$  subtracted singles spectra. There is a shoulder on the low excitation energy side of the  $^{64}\text{Zn}$  GQR peak which may be due to incomplete subtraction of the  $^{12}\text{C}$  9.6 MeV  $3^-$  state. Also, the continuum is slightly larger in the  $^{64}\text{Zn}$  spectrum than that observed for the heavier isotopes. Results

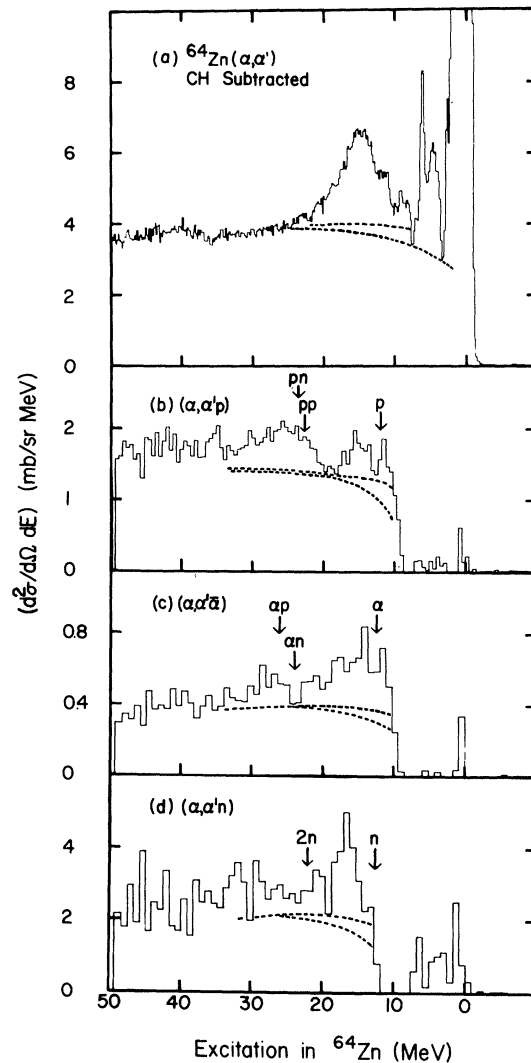


FIG. 2. (a) The inelastic alpha particle spectrum at  $14^\circ$  for the reaction  $^{64}\text{Zn}(\alpha, \alpha')^{64}\text{Zn}$  at 160 MeV. The same spectrum is also shown subject to the requirement of (b) a proton, (c) an alpha particle, or (d) a neutron coincidence in a second detector. These spectra represent an integration over decay particle angles and have been corrected for a small amount of carbon-hydrogen contamination. The effective one particle and lowest multiparticle emission thresholds in  $^{64}\text{Zn}$  are indicated in (b)–(d). Maximum and minimum estimates of the continuum backgrounds are shown as dashed lines.

from 129 MeV inelastic alpha particle scattering from  $^{64}\text{Zn}$  and  $^{66}\text{Zn}$  provide evidence for the presence of a giant monopole resonance (GMR) component in the high excitation energy side of the GQR peak.<sup>25</sup> The possible presence of a small amount of GMR strength in the GQR region of Zn

has been neglected in the present analysis.

The extraction of the GQR cross section is complicated by the ambiguity in determining the shape of the nuclear continuum beneath it. This continuum background shape has been estimated by interpolation between the regions on either side of the resonance peak. These estimates are shown as dashed lines in the figures. The GQR singles yield above this continuum [Figs. 2(a), 3(a), and 4(a)] is thus determined to be  $14 \pm 2$ ,  $13.5 \pm 1.5$ , and  $13 \pm 1$  mb/sr for  $^{64}\text{Zn}$ ,  $^{66}\text{Zn}$ , and  $^{68}\text{Zn}$ , respectively. The uncertainties are obtained by extracting the GQR yields with the maximum and minimum possible background estimates that are consistent with the data. The respective peak to background ratios are 1/3.4, 1/2.8, and 1/2.8.

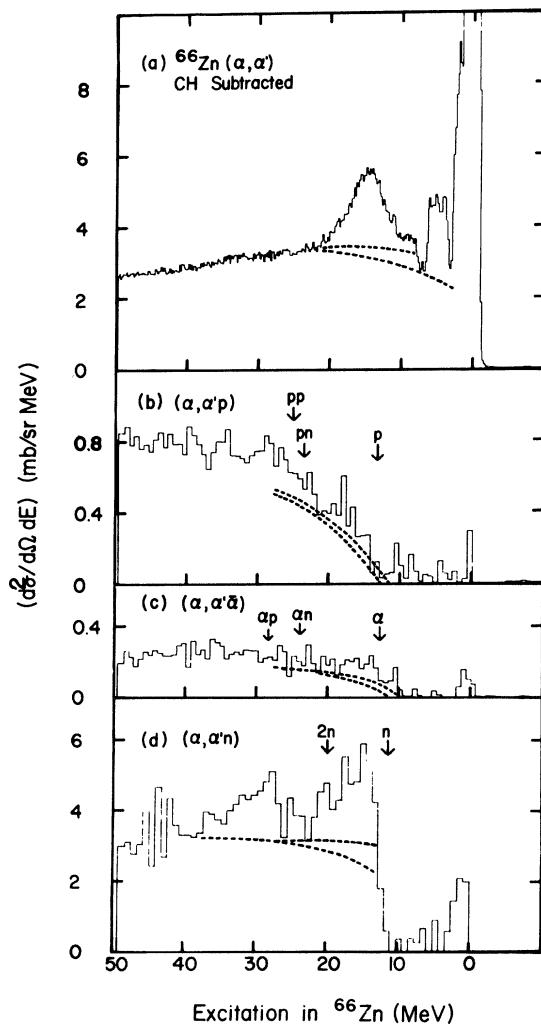


FIG. 3. The CH subtracted singles and particle-particle coincidence spectra of  $^{66}\text{Zn}$ , as in Fig. 2.

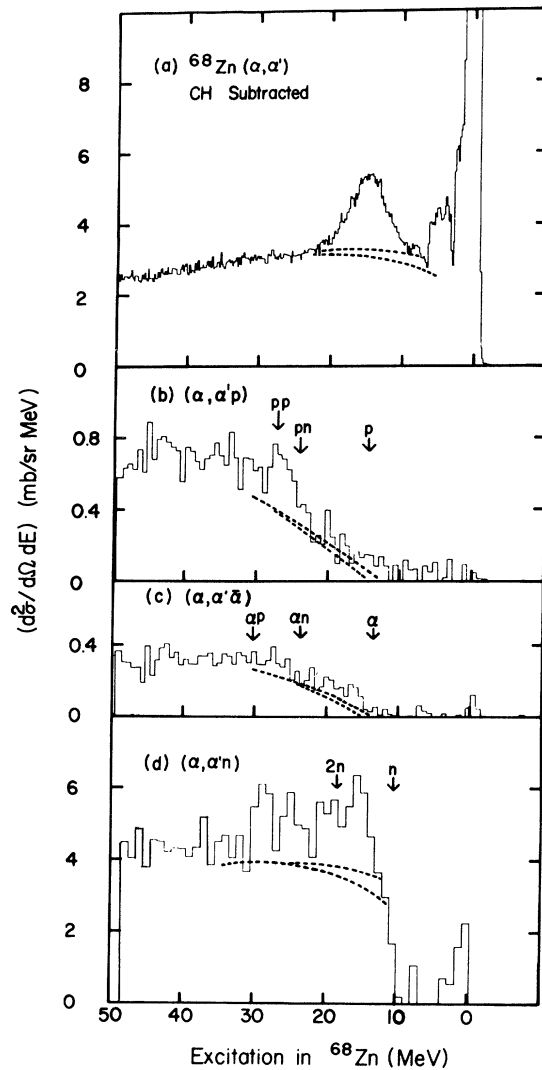


FIG. 4. The CH subtracted spectra of  $^{68}\text{Zn}$ , as in Fig. 2.

Parts (b)–(d) of Figs. 2–4 show the inelastic alpha particle spectrum with the requirement of a proton, alpha particle, or neutron coincidence in a decay particle detector, respectively. These coincidence spectra represent angular integrations over decay particle detectors and may be directly compared with the singles spectra. It is assumed that the distribution of decay products is axially symmetric about the Zn GQR recoil direction in the center-of-mass system of the recoiling excited nucleus. However, recoil center-of-mass effects for the Zn nuclei were only of the order of 10% and therefore all integrations have been performed in the laboratory system. As with the singles spectra, the corresponding angle-integrated coincidence spectra

from a CH target have been subtracted from the Zn coincidence spectra to correct for a small amount of contamination. The main effect of the subtractions was to reduce the alpha particle decay yield from  $^{64}\text{Zn}$  by about 20% in the excitation energy region above 15 MeV.

The  $^{64}\text{Zn}$  and  $^{66}\text{Zn}$  charged particle coincidence spectra represent an integration over eight decay particle angles (see Table I). These angles were approximately evenly spaced between the GQR recoil and opposite recoil directions, within the reaction plane. The  $^{68}\text{Zn}$  charged particle coincidence spectra were derived from four decay angles (see Table I). Contributions from charged particles stopping in the decay  $\Delta E$  detectors were negligible and not included in the integrated coincidence spectra. All neutron coincidence spectra were obtained by integrating over the two coincidence angles defined by the NE-102 counter, about  $-60^\circ$  and  $160^\circ$  relative to the Zn GQR recoil direction. Absolute cross sections have been obtained by dividing by the estimated 54% neutron detector efficiency.

The  $^{64}\text{Zn}$  coincidence spectra of Fig. 2 all exhibit an enhanced yield above the estimated continuum background (dashed lines) in the region of excitation of the GQR which can be associated with the particle decay of the resonance. The coincidence spectra of Fig. 3 show that the decay charged particle yield from  $^{66}\text{Zn}$  is greatly reduced relative to that from  $^{64}\text{Zn}$ . There is little if any yield above the continuum background that would correspond to proton or alpha particle decay of the GQR in  $^{66}\text{Zn}$ . Most of the decay strength is observed in the neutron coincidence spectrum. The  $^{68}\text{Zn}$  particle coincidence spectra of Fig. 4 continue the trends observed for  $^{66}\text{Zn}$ . Practically no proton yield and very little alpha particle yield exist in the GQR region of  $^{68}\text{Zn}$ . The neutron yield dominates.

TABLE I. Angles of observation for decay charged particles in the laboratory system. The inelastically scattered alpha particles were detected at  $\theta_{\text{lab}} = +14^\circ$ .

Target	Angles of observation			
$^{64}\text{Zn}$	$\pm 40^\circ$	$\pm 80^\circ$	$\pm 120^\circ$	$\pm 160^\circ$
$^{66}\text{Zn}$	$\pm 40^\circ$	$\pm 80^\circ$	$\pm 120^\circ$	$\pm 160^\circ$
$^{68}\text{Zn}$	$\pm 40^\circ$			$\pm 160^\circ$

Other features of the coincidence spectra are best understood in terms of the effective particle emission thresholds. The excitation energies corresponding to the effective one particle and lowest multiparticle emission thresholds are indicated in Figs. 2–4. Each single charge particle effective threshold is defined here to be the particle separation energy plus the height of the Coulomb barrier. The shapes of the energy spectra of the decay particles are characteristic of a particle evaporation process (see Fig. 5). The Coulomb barrier height was estimated from the maxima in the decay charged particle spectra to be 4.3 MeV for protons and 8.2 MeV for alpha particles. The neutron emission threshold is the sum of the separation energy and the height of the angular momentum barrier. This barrier was below the lower experimental cutoff in the neutron energy spectrum (about 0.6 MeV) and it was assumed to be about 0.5 MeV. Each multiparticle effective threshold is the sum of the appropriate separation energy and the barrier height for each particle.

Yield is seen in all of the coincidence spectra down to excitation energies near the effective one

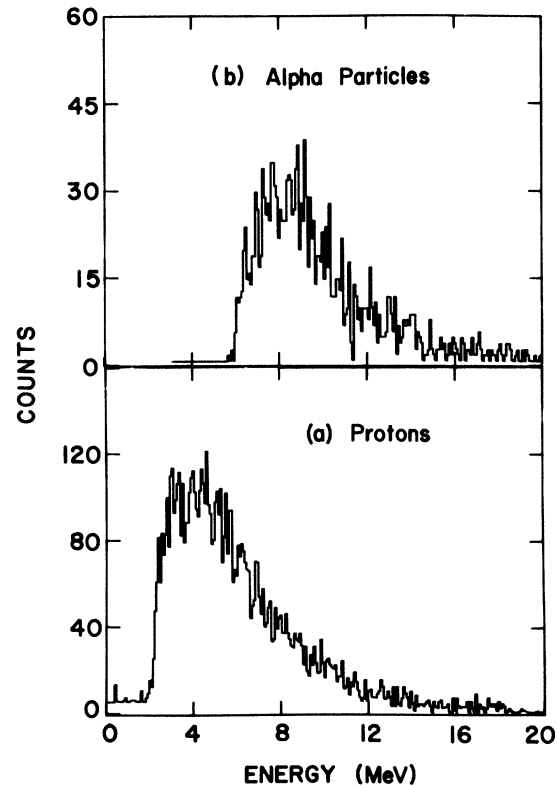


FIG. 5. (a) Proton and (b) alpha particle decay energy spectra from  $^{64}\text{Zn}$ .

particle thresholds, as expected. In some cases, high effective particle thresholds inhibit particle emission from the low excitation energy side of the GQR peak. The presence of counts in the excitation region of the Zn discrete states is due to statistical fluctuations which lead to imperfect random coincidence subtraction. The small number of these counts indicates that the random subtraction is adequate for the purposes of the experiment.

Particle emission from the region of excitation between the effective one particle and two particle emission thresholds is limited to a single nucleon or alpha particle, neglecting gamma ray competition. In this region, the sum of the proton, neutron, and alpha particle yields should equal that of the singles yield. The sum of the coincidence yields in the excitation energy range of 15–17 MeV is found to account for 100% of the singles yield, within experimental uncertainties. This also confirms the calculated neutron detector efficiency that was used in the normalization of the neutron coincidence spectra.

In the region of excitation above the effective two particle thresholds the emitted particle multiplicity is expected to be greater than one. The sum of the coincidence yields may then exceed that of the singles yield. This is especially apparent in the neutron decay yields from  $^{66}\text{Zn}$  and  $^{68}\text{Zn}$ , each of which is larger than its respective singles yield above the  $2n$  threshold. In fact, the  $2n$  effective threshold in  $^{68}\text{Zn}$  is low enough to allow multiple neutron emission

from the high excitation energy side of the GQR peak. Also, a secondary bump is seen in some of the nucleon decay coincidence spectra above the GQR region which is not seen in the singles spectra. These structures seem to be associated with the multiparticle effective threshold. They probably reflect an increase in particle multiplicity at energies where one or more strong two particle emission channels open followed by a decrease in multiplicity with the onset of similar processes in other channels. The presence of such competing channel effects complicates the extraction of the GQR decay yields.

The Zn GQR yields from the angle integrated coincidence spectra were obtained, as for the singles yields, by summing the counts above maximum and minimum estimated continuum backgrounds. The results for the particle decay branching ratios of each Zn GQR and the continuum background beneath it are summarized in Table II. The combined error estimates from the singles and coincidence yields are given. The uncertainties in the neutron branching ratios are dominated by the estimated uncertainty in the neutron detector efficiency. The values of the charged particle decay branches have about 20% errors for the GQR and about 10% errors for the background. The uncertainties in the neutron decay branches are all of the order of 40%. The measured total particle decay strength for each Zn isotope accounts for 100% of the singles GQR cross section. However, the large uncertainties leave room for the possibility of gam-

TABLE II. Experimental decay branches and statistical model predictions.

Nucleus	Decay particle	Experimental		Calculated Hauser-Feshbach	
		GQR	Underlying continuum	$J^\pi = 2^+$	all $J^\pi$
$^{64}\text{Zn}$	$p$	38 $\pm$ 7	24 $\pm$ 2	46	43
	$n$	59 $\pm$ 27	58 $\pm$ 23	28	34
	$\alpha$	20 $\pm$ 4	9.3 $\pm$ 1.2	26	23
$^{66}\text{Zn}$	$p$	4.4 $\pm$ 1.6	7.4 $\pm$ 0.4	6	5
	$n$	113 $\pm$ 45	88 $\pm$ 34	86	91
	$\alpha$	3.7 $\pm$ 0.9	3.7 $\pm$ 0.4	8	4
$^{68}\text{Zn}$	$p$	0.8 $\pm$ 0.8	4.6 $\pm$ 0.4	1	1
	$n$	124 $\pm$ 51	111 $\pm$ 43	96	97
	$\alpha$	3.1 $\pm$ 0.8	2.6 $\pm$ 0.2	3	2

ma ray decay. This is especially true on the low excitation energy side of each Zn GQR peak, where the total particle decay strength seen in the coincidence spectra seems to fall short of the yield in the singles spectrum.

The statistical model prediction of a shift from charged particle to neutron GQR decay with increasing neutron excess in Zn is seen in the measured branching ratios. Also, the decay branches of the GQR and the underlying continuum for each isotope are generally similar. The coincidence spectra themselves exhibit a clear dependence on the positions of the various effective particle emission thresholds. These results confirm the importance of statistical effects in the decay of the GQR in medium mass nuclei.

#### IV. DISCUSSION

A comparison of the experimentally measured branching ratios with Hauser-Feshbach calculations provides an indication of the extent to which the GQR decay is influenced by statistical processes. The Hauser-Feshbach spin dependent formulation of compound nucleus reaction theory predicts the relative average cross sections for the statistical decay of a fused target plus projectile system.<sup>26</sup> For the purpose of calculating the decay of the GQR in a given target, the resonance has been assumed to be formed by proton capture into the GQR on the  $(Z - 1, A - 1)$  target. The results depend only on nuclear transmission factors, level densities,  $Q$  values, and the conservation laws.

The statistical model calculations have been made with the computer code STATIS.<sup>27</sup> The program obtains transmission factors and spin dependent level densities from rough parametrizations. The experimental energies and spins of the lowest few known states of each residual nucleus were used in the calculations. The empirical level density formula was used for the region of excitation above these states with a level density parameter of  $a = A/8$  MeV<sup>-1</sup>. Table II shows the calculated branching ratios for a  $2^+$  state at the GQR excitation energy in each Zn isotope as well as for a sum over all  $J^\pi$  at that energy. One would expect that if the GQR decays statistically, its decay branches should be predicted by the Hauser-Feshbach calculation for  $J^\pi = 2^+$ . The continuum decay branches should contain contributions from many different spins. They should be comparable with the results which are summed over  $J^\pi$ . It is clear from the table that the calculations for a  $2^+$  state are about the same as those averaged over  $J^\pi$ .

The measured values for the Zn GQR and the underlying continuum decay branches are in general agreement with the statistical model predictions. The small experimental continuum proton yield in <sup>68</sup>Zn is larger than the calculated value by much more than the estimated empirical uncertainty. The charged particle continuum yield in <sup>64</sup>Zn is significantly less than calculated. The measured neutron branches are generally higher than the predictions, but they are still in agreement within the rather large uncertainties. In some cases the measured values for the neutron decay branches exceed 100%. This may be due in part to possible multiple neutron emission from the high excitation energy side of the GQR region.

It should be noted in this comparison that the statistical model calculations contain uncertainties in that they use some parametrizations for quantities rather than the measured values for each nucleus. However, these effects should be small relative to the experimental uncertainties since the model is used only to calculate the relative decay strengths and not absolute cross sections. Within the accuracy of the data and the calculations, the particle decay of the GQR in the three Zn isotopes studied appears to be predominantly statistical in nature.

A systematic picture of the GQR decay properties is beginning to emerge from the coincidence experiments that have been performed to date. These have generally employed inelastic alpha particle scattering, for which the GQR is the most prominent giant resonance to be excited. A review of the coincidence experiments has been given by Wagner.<sup>21</sup> It has been shown that essentially no GQR exists in <sup>12</sup>C,<sup>12</sup> establishing a lower mass limit on the observation of the resonance. The GQR that is seen in such nuclei as <sup>16</sup>O and <sup>28</sup>S has a somewhat larger alpha particle decay branch than statistical model predictions and little proton decay is seen.<sup>10,11</sup>

However, a large GQR proton decay and small alpha particle decay are observed from <sup>40</sup>Ca (Ref. 17) and <sup>58</sup>Ni,<sup>18</sup> which are compatible with Hauser-Feshbach calculations. It is inferred from a lack of charged particle decay that neutron emission is the most important GQR decay channel in <sup>62</sup>Ni.<sup>20</sup> The present work shows that single nucleon emission is found to dominate the GQR decay of <sup>64</sup>Zn and neutron emission is the overwhelming GQR decay mode in <sup>66</sup>Zn and <sup>68</sup>Zn. These results are also in agreement with a statistical model of the decay process. While the GQR may not be compact and observable in the lightest systems and seems to have

nonstatistical components in light nuclei, the experiments between  $^{40}\text{Ca}$  and  $^{68}\text{Zn}$  show strong evidence of statistical decay. The only other GQR coincidence experiments that have been performed so far are in the mass range  $A > 200$  and the results for heavy nuclei are still unclear. For example, one group reports that no GQR peak is seen in the fission coincidence spectrum of  $^{238}\text{U}$ ,<sup>22</sup> while another group finds a very structured spectrum.<sup>23</sup>

It is interesting to note that a recent shell model calculation by Faessler *et al.*,<sup>28</sup> which includes predominately 1p-1h excitations, predicts the details of the  $^{16}\text{O}$  GQR decay fairly well and is consistent with results for the  $^{40}\text{Ca}$  GQR decay. However, the measurements of Ref. 17 set only an upper limit on the ratio of the alpha particle to proton decay of the GQR in  $^{40}\text{Ca}$ . While statistical model calculations underestimate this ratio by about a factor of 2.5 in the case of  $^{16}\text{O}$ , they are, like the shell model calculations, also consistent with the  $^{40}\text{Ca}$  results.<sup>18,21</sup>

The experimental situation of the GQR decay in  $^{58}\text{Ni}$  has been greatly clarified within the last year. Hayward has reported that a virtual photon spectrum analysis of charged particle electroproduction data from  $^{58}\text{Ni}$  (Ref. 29) that yielded an essentially 100% GQR alpha particle decay branch has been redone.<sup>30</sup> The alpha particle branch has been reduced by more than a factor of 3, but the GQR proton decay strength remains unmeasurable. The same type of experiment and analysis have been performed on  $^{58}\text{Ni}$  at Glasgow<sup>31</sup> and these results are consistent with the 59% proton and 12% alpha particle GQR decay branches found in our previous coincidence work.<sup>18</sup> A second coincidence experiment has been done by Knöpfle *et al.*, in which GQR decay branches are found of 65% for the proton channel and less than 30% for the alpha particle channel.<sup>19</sup> Finally, the results of a recent coupled channels calculations for low energy alpha particle scattering on  $^{54}\text{Fe}$  are found to be consistent with a 12%  $^{58}\text{Ni}$  GQR alpha particle decay branch.<sup>32</sup> It now appears that the results of the coincidence experiments are well established, and in agreement with a statistical decay process.

The width of a giant resonance is related to its decay properties in that it consists of the sum of the escape width and the spreading (or damping) width. The escape width  $\Gamma^\dagger$  is due to the coupling of the resonance to the continuum, while  $\Gamma^\ddagger$ , the spreading width, is due to the coupling to nuclear states which are more complicated than the initial 1p-2h configurations. If the coupling of the resonance to the

complex multiparticle, multihole states is strong, the nucleus will equilibrate and its decay will be characteristic of a compound nucleus. If a strong coupling to the continuum exists, the resonance will decay by direct particle emission. Otherwise, the decay properties will fall somewhere between these two extremes. Without a detailed knowledge of the wave function for the GQR, the interplay between direct particle emission and equilibrium may be partially understood in the context of a preequilibrium exciton model calculation. This model has been used to account for the high energy continuum spectra seen in medium and high energy projectile scattering.<sup>33,34</sup> In the following, the exciton model will be used to estimate the escape and spreading widths as a function of nuclear mass.

In the preequilibrium exciton model,<sup>35,36</sup> a projectile and target are treated as a composite system formed in a specific particle-hole state after their first nuclear interaction. The particular initial state depends, in general, on the projectile. The system is then allowed to proceed to more complicated multiparticle, multihole states via energy conserving two-body residual interactions. Each step in the reaction is characterized by the exciton number (the number of particles and holes excited) and by the excitation energy. At each stage, the system is allowed to create or destroy a particle-hole pair or decay by particle emission. In the exciton model formalism, the widths for these three processes are  $\Gamma_+$ ,  $\Gamma_-$ , and  $\Gamma_c$ , respectively. They are defined as a function of the particle number ( $p$ ), the hole number ( $h$ ), and the excitation energy. At any stage in the process, the total width is equal to

$$\Gamma(p, h, E) = \Gamma_+(p, h, E) + \Gamma_-(p, h, E) + \Gamma_c(p, h, E).$$

The spreading width of a configuration,  $\Gamma^\ddagger$ , is identified with  $\Gamma_+$  and the escape width  $\Gamma^\dagger$  is equal to  $\Gamma_c$ . The total width is essentially equal to  $\Gamma_+ + \Gamma_c = \Gamma^\ddagger + \Gamma^\dagger$  in the early stages of the equilibration process because  $\Gamma_-$  is usually negligible. The system is considered to be equilibrated when the particle-hole pair creation rate equals the annihilation rate,  $\Gamma_+ = \Gamma_-$ . Any further particle emission then occurs through an evaporation process.

The initial configuration of the GQR in the exciton model is a 1p-1h state of the target nucleus with an excitation energy equal to the resonance centroid energy. Preequilibrium model estimates of the ratio of the GQR escape width to the total width  $\Gamma$  for various nuclei from  $^{12}\text{C}$  to  $^{209}\text{Bi}$  are shown in Table



TABLE III. Preequilibrium estimates of the GQR escape widths for various nuclei.

Nucleus	GQR excitation energy (MeV)	Binding energies			$(\Gamma'/\Gamma)$ 1p-1h (%)	$(\Gamma'/\Gamma)$ up to 4p-4h (%)
		<i>n</i>	<i>p</i>	$\alpha$		
<sup>12</sup> C	27.5	18.719	15.956	7.368	21	43
<sup>16</sup> O	21	15.666	12.112	7.152	17	33
<sup>20</sup> Ne	23.2	16.857	12.835	4.733	15	41
<sup>24</sup> Mg	21.8	16.530	11.683	9.310	13	20
<sup>26</sup> Mg	21.3	11.086	14.128	10.603	20	32
<sup>27</sup> Al	21	13.304	8.258	10.077	21	35
<sup>28</sup> Si	20.7	17.155	11.570	9.964	9	12
<sup>32</sup> S	19.8	15.080	8.855	6.950	13	20
<sup>40</sup> Ca	18.4	15.620	8.315	7.036	9	12
<sup>58</sup> Ni	16.3	12.181	8.173	6.396	6	7
<sup>62</sup> Ni	19.9	10.589	11.101	7.021	7	8
<sup>64</sup> Zn	15.75	11.840	7.689	3.951	6	7
<sup>66</sup> Zn	15.59	11.030	8.898	4.548	6	7
<sup>68</sup> Zn	15.43	10.191	9.978	5.302	7	8
<sup>90</sup> Zr	14.1	11.982	8.372	6.680	1	1
<sup>209</sup> Bi	10.6	7.434	3.781	-3.127	3	3

III. They were calculated with the program PREQEC (see Appendix C of Ref. 37) using an initial 1p-1h configuration at the GQR excitation energy in each nucleus.

The table shows the results for the initial 1p-1h configuration and the contributions up to the 4p-4h stage of the calculation. The calculated ratios for the 1p-1h through the 3p-3h step are essentially the same and represent single nucleon emission. There is an increase in  $(\Gamma'/\Gamma)$  at the 4p-4h step, especially for the lighter nuclei, because alpha particle emission becomes possible when four or more particles are excited. There is then little change in  $(\Gamma'/\Gamma)$  beyond the 4p-4h stage.

The exciton model calculation predicts that direct particle emission will provide a 30–40% contribution to the total GQR width for nuclei of mass  $A < 28$ . This contribution decreases with increasing mass down to values of only a few percent for <sup>90</sup>Zr and <sup>209</sup>Bi. It is less than 9% for any of the nuclei with mass  $A > 40$  for which  $(\Gamma'/\Gamma)$  was computed. Comparison of the 1p-1h results with the 4p-4h values shows that direct alpha particle emission is competitive with direct nucleon emission in the lighter nuclei and that it becomes insignificant for the heavier ones. This is consistent with measured

branching ratios. In the case of the Zn isotopes, direct particle emission is predicted to contribute about 7% to the total GQR width. In summary, the preequilibrium exciton model predicts that direct and statistical particle emission are comparable in light nuclei. However, in the mass range  $A > 40$ , direct particle emission is suppressed by more than a factor of 10 relative to statistical processes.

It should be noted that the exciton model calculations described above use an unrealistic equal-spacing model for the nuclear level density. Also, the model uses a simple 1p-1h initial configuration for the GQR state even though the resonance is a superposition of many 1p-1h states. It has been suggested by Luk'yanov<sup>38</sup> that the collective nature of the GQR could be treated by using an effective initial 1p-1h state density which is much larger than the normal values. This would tend to enhance direct particle emission, but an effective 1p-1h state density has not been incorporated into the calculations presented here. Nevertheless, these model calculations provide an indication of the relative importance of direct and statistical decay of the GQR as a function of nuclear mass. They are also consistent with the experimental observations.

## V. CONCLUSION

A direct particle-particle coincidence experiment has been performed to look for the strong isotopic (particle emission threshold) dependence of the GQR particle decay in Zn which is predicted by Hauser-Feshbach calculations. The total GQR proton, neutron, and alpha particle decay branching ratios have been measured on  $^{64}\text{Zn}$ ,  $^{66}\text{Zn}$ , and  $^{68}\text{Zn}$ . They are similar to those of the underlying continuum and to statistical model predictions, within the experimental uncertainties. The Zn coincidence spectra also exhibit a dependence on particle emission thresholds and barriers and on particle multiplicities. The results indicate a strong statistical influence on the particle decay from the entire GQR region of excitation in the Zn isotopes.

Other coincidence studies have shown evidence for a large, nonstatistical GQR alpha particle decay from light systems, such as  $^{16}\text{O}$  (Ref. 10) and  $^{28}\text{Si}$ .<sup>11</sup> However, work on  $^{40}\text{Ca}$  (Ref. 17) and on  $^{58}\text{Ni}$  (Ref. 18) show a large GQR proton decay which is compatible with a statistical model interpretation. The results of the present Zn experiment show that single nucleon emission accounts for most of the GQR decay from  $^{64}\text{Zn}$  and that the GQR in  $^{66}\text{Zn}$  and  $^{68}\text{Zn}$  decays almost exclusively by neutron emission. This is also in qualitative agreement with statistical model predictions. GQR decay experiments have been performed recently in the mass region of  $A > 200$ , but some of these results are contradictory at the present time.<sup>21-23</sup> The trend observed in the light mass region is for the strong GQR alpha

particle decay to give way to single nucleon emission with increasing mass. It has been shown that this is in agreement with the predictions of the pre-equilibrium exciton model. The exciton model calculations also indicate that statistical GQR particle emission is favored over direct emission by about a factor of 10 for nuclei of mass  $A > 40$ . The total width of the GQR in this mass region is therefore largely a damping width, consistent with the observed statistical decay.

The presence of direct GQR particle decay components in the light nuclei may yet provide detailed information on the initial 1p-1h configurations which make up the GQR state. If the dominance of the statistical GQR decay seen in heavier elements is confirmed throughout the rest of the mass range, the simple 1p-1h GQR structure will be obscured because it is strongly coupled to more complex particle-hole states. In this case, the isoscalar GQR will be seen as the initial stage of an energy dissipation mechanism in which the energy of the collective GQR vibration is spread into many complex nuclear degrees of freedom.

## ACKNOWLEDGMENTS

A grant from the University of Maryland Computer Science Center for use in performing some of the calculations is acknowledged. This work was supported in part by the National Science Foundation and is based on an unpublished dissertation (M.T.C.) in partial fulfillment of the requirements for the Ph.D. degree in Physics.

\*Present address: Brookhaven National Laboratory, Upton, N. Y. 11973.

†Present Address: Physics Dept., Florida State University, Tallahassee, Florida 32306.

<sup>1</sup>R. Pittham and T. Walcher, *Phys. Lett.* **36B**, 563 (1971).

<sup>2</sup>M. B. Lewis and F. E. Bertrand, *Nucl. Phys.* **A196**, 337 (1972).

<sup>3</sup>C. C. Chang, F. E. Bertrand, and D. C. Kocher, *Phys. Rev. Lett.* **34**, 221 (1975).

<sup>4</sup>A. Moalem, W. Benenson, and G. M. Crawley, *Phys. Rev. Lett.* **31**, 482 (1973).

<sup>5</sup>D. H. Youngblood *et al.*, *Phys. Rev. C* **13**, 994 (1976).

<sup>6</sup>H. J. Gils, H. Rebel, J. Buschman, and H. Klewe-Nebenius, *Phys. Lett.* **68B**, 427 (1977).

<sup>7</sup>R. Betts, S. DiCenzo, M. Mortensen, and R. White, *Phys. Rev. Lett.* **39**, 1183 (1977).

<sup>8</sup>P. Doll *et al.*, *Phys. Rev. Lett.* **42**, 366 (1979).

<sup>9</sup>J. Arvieux *et al.*, *Phys. Rev. Lett.* **42**, 749 (1979).

<sup>10</sup>K. T. Knöpfle *et al.*, in *Lecture Notes in Physics*, edited by B. A. Robson (Springer, Berlin, 1979), Vol. **92**, p. 443.

<sup>11</sup>K. T. Knöpfle *et al.*, *Phys. Lett.* **74B**, 191 (1978).

<sup>12</sup>H. Riedesel *et al.*, *Phys. Rev. Lett.* **41**, 377 (1978).

<sup>13</sup>J. R. Nix and A. J. Sierk, *Phys. Rev. C* **21**, 396 (1980), and references therein.

<sup>14</sup>J. S. Dehesa, S. Krewald, J. Speth, and A. Faessler, *Phys. Rev. C* **15**, 1858 (1977).

<sup>15</sup>S. Shlomo and G. Bertsch, *Nucl. Phys.* **A243**, 507 (1975).

<sup>16</sup>K. F. Liu and G. E. Brown, *Nucl. Phys.* **A265**, 385 (1976).

<sup>17</sup>D. H. Youngblood *et al.*, *Phys. Rev. C* **15**, 246 (1977).

<sup>18</sup>M. T. Collins *et al.*, *Phys. Rev. Lett.* **42**, 1440 (1979).

<sup>19</sup>K. T. Knöpfle *et al.*, in *Lecture Notes in Physics*, edited by B. A. Robson (Springer, Berlin, 1979), Vol. **92**, p. 444.

<sup>20</sup>K. T. Knöpfle, in *Lecture Notes in Physics*, edited by

- H. Arenhövel and D. Drechsel (Springer, Berlin, 1979), Vol. 108, p. 311.
- <sup>21</sup>G. J. Wagner, in *Proceedings of the Giant Multipole Resonance Topical Conference, Tennessee (1979)*, edited by F. E. Bertrand (Academic, New York, 1979), p. 251.
- <sup>22</sup>J. van der Plicht *et al.*, *Phys. Rev. Lett.* 42, 1121 (1979).
- <sup>23</sup>A. C. Shotton *et al.*, *Phys. Rev. Lett.* 43, 569 (1979).
- <sup>24</sup>R. A. Cecil, B. D. Anderson, and R. Madey, *Nucl. Instrum. Methods* 161, 439 (1979).
- <sup>25</sup>Y.-W. Lui *et al.*, *Phys. Lett.* 93B, 31 (1980).
- <sup>26</sup>H. Feshbach, Sec. V. A. in *Nuclear Spectroscopy, Part B*, edited by F. Ajzenberg-Selove (Academic, New York, 1960), p. 625.
- <sup>27</sup>R. Stokstad, (unpublished).
- <sup>28</sup>A. Faessler, D. J. Millener, P. Paul, and D. Strottman, *Nucl. Phys.* A330, 333 (1979).
- <sup>29</sup>E. Wolyneć, W. R. Dodge, and E. Hayward, *Phys. Rev. Lett.* 42, 27 (1979).
- <sup>30</sup>E. Hayward, in *Proceedings of the Giant Multipole Resonance Topical Conference, Tennessee (1979)*, edited by F. E. Bertrand (Academic, New York, 1979), p. 275.
- <sup>31</sup>J. C. McGeorge, A. G. Flowers, D. Branford, and C. H. Zimmerman (unpublished).
- <sup>32</sup>D. P. Stanley and D. Halderson, *Phys. Rev. C* 20, 2114 (1979).
- <sup>33</sup>J. R. Wu, C. C. Chang, and H. D. Holmgren, *Phys. Rev. C* 19, 659 (1979).
- <sup>34</sup>J. R. Wu, C. C. Chang, and H. D. Holmgren, *Phys. Rev. C* 19, 370 (1979); 19, 698 (1979).
- <sup>35</sup>J. R. Wu and C. C. Chang, *Phys. Lett.* B60, 423 (1976).
- <sup>36</sup>J. R. Wu and C. C. Chang, *Phys. Rev. C* 16, 1812 (1977).
- <sup>37</sup>J. R. Wu, Ph.D. thesis, University of Maryland, 1977 (unpublished).
- <sup>38</sup>V. K. Luk'yanov, V. A. Seliverstov, and V. D. Toneev, *Yad. Fiz.* 21, 992 (1975) [*Sov. J. Nucl. Phys.* 21, 508 (1975)].